All-pass Parametric Image Registration

Supplementary Material

Xinxin Zhang, *Student Member, IEEE,* Christopher Gilliam, *Member, IEEE,* and Thierry Blu, *Fellow, IEEE*

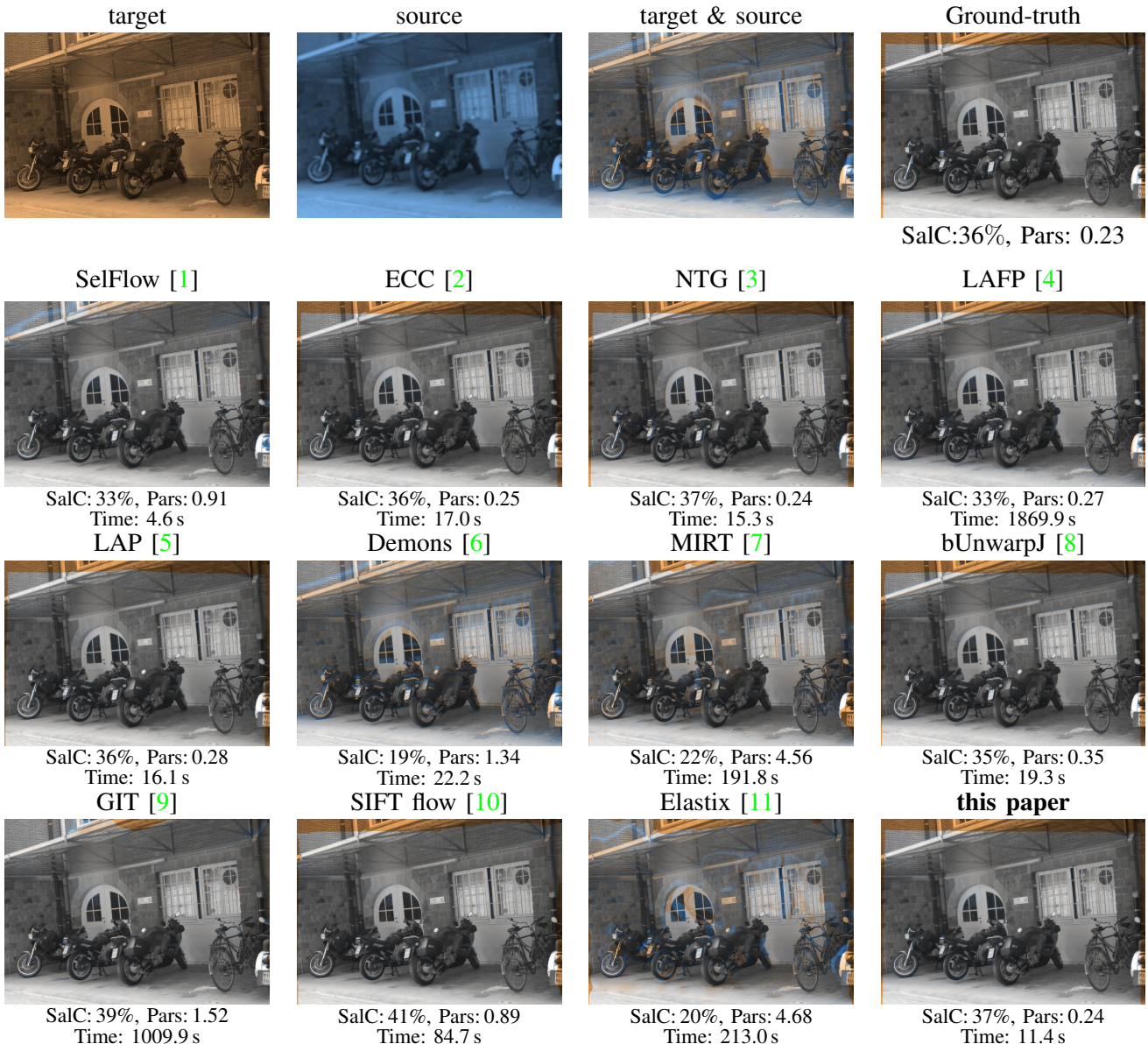

Fig. S1. Results of our algorithm on the Oxford affine dataset [12]–the subset of "Bikes" (700 × 1000 pixels): alignment of the last image (i.e., the most distorted one: worst case) of each of the three subsets with the first image.

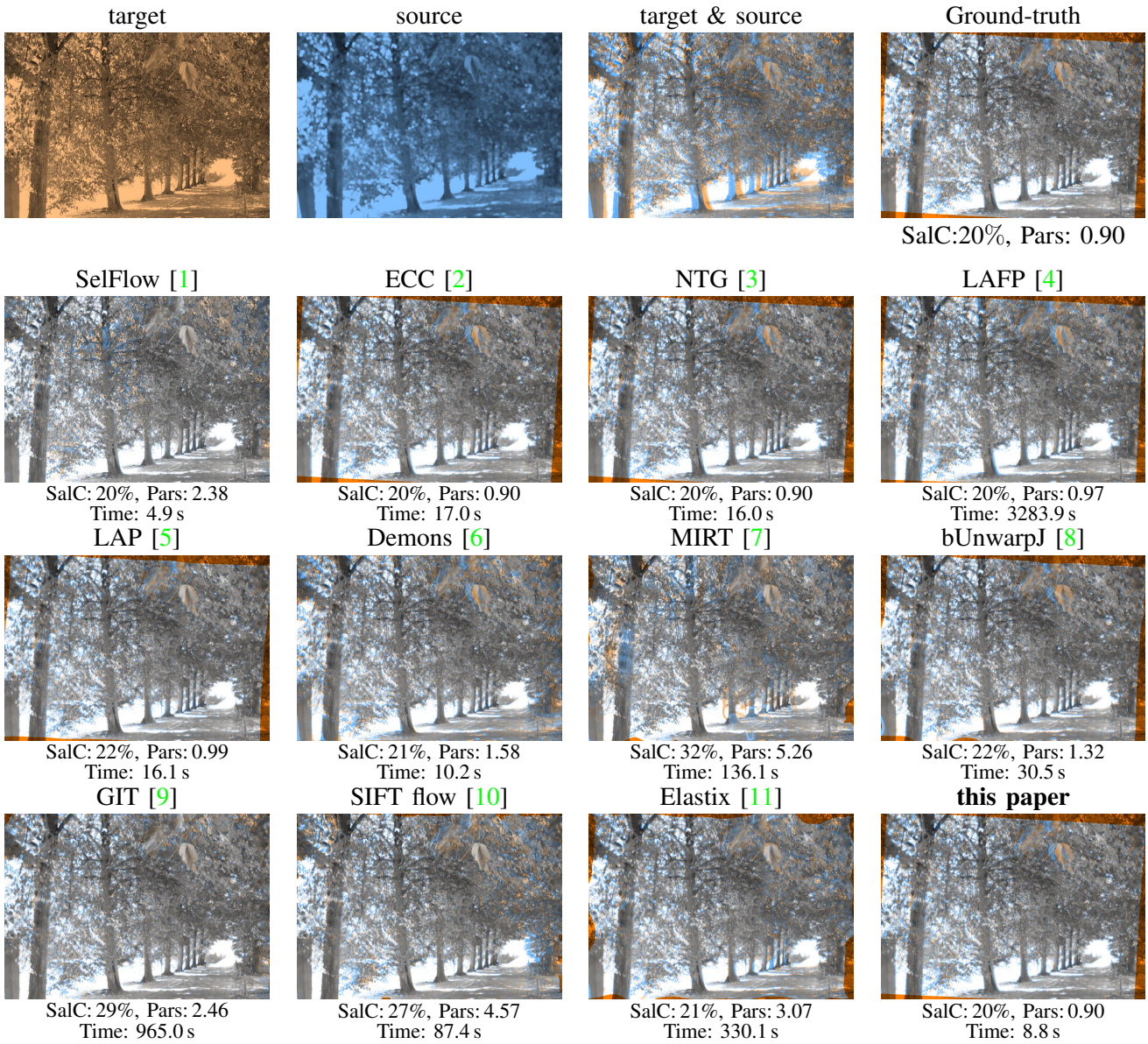

Fig. S2. Results of our algorithm on the Oxford affine dataset [12]–the subset of "Trees" (700 × 1000 pixels): alignment of the last image (i.e., the most distorted one: worst case) of each of the three subsets with the first image. Although the SalC of the MIRT algorithm is much larger than that of the ground-truth, the large parsimony indicates that the displacement is incorrect.

REFERENCES

[1] P. Liu, M. Lyu, I. King, and J. Xu, "Selflow: Self-supervised learning of optical flow," in *Proceedings of the IEEE Conference on Computer Vision and Pattern Recognition*, 2019, pp. 4571–4580.

[2] G. D. Evangelidis and E. Z. Psarakis, "Parametric image alignment using enhanced correlation coefficient maximization," *IEEE Transactions on Pattern Analysis and Machine Intelligence*, vol. 30, pp. 1858–1865, 2008.

[3] S.-J. Chen, H.-L. Shen, C. Li, and J. H. Xin, "Normalized total gradient: a new measure for multispectral image registration," *IEEE Transactions on Image Processing*, vol. 27, no. 3, pp. 1297–1310, 2018.

[4] Y. Matsushita, "Aligning images in the wild," in *IEEE Conference on Computer Vision and Pattern Recognition (CVPR)*, 2012, pp. 1–8.

[5] C. Gilliam and T. Blu, "Local all-pass geometric deformations," *IEEE Transactions on Image Processing*, vol. 27, no. 2, pp. 1010–1025, 2018.

[6] H. Lombaert, L. Grady, and X. P. *et al.*, "Diffeomorphic demons: Efficient non-parametric image registration," *NeuroImage*, vol. 45, pp. S61–S72, 2009.

[7] A. Myronenko and X. Song, "Intensity-based image registration by minimizing residual complexity," *IEEE Transactions on Medical Imaging*, vol. 29, pp. 1882–1891, 2010.

[8] I. Arganda-Carreras, C. O. S. Sorzano, and R. M. *et al.*, "Consistent and elastic registration of histological sections using vector-spline regularization," in *International Workshop on Computer Vision Approaches to Medical Image Analysis (CVAMIA)*, 2006, pp. 85–95.

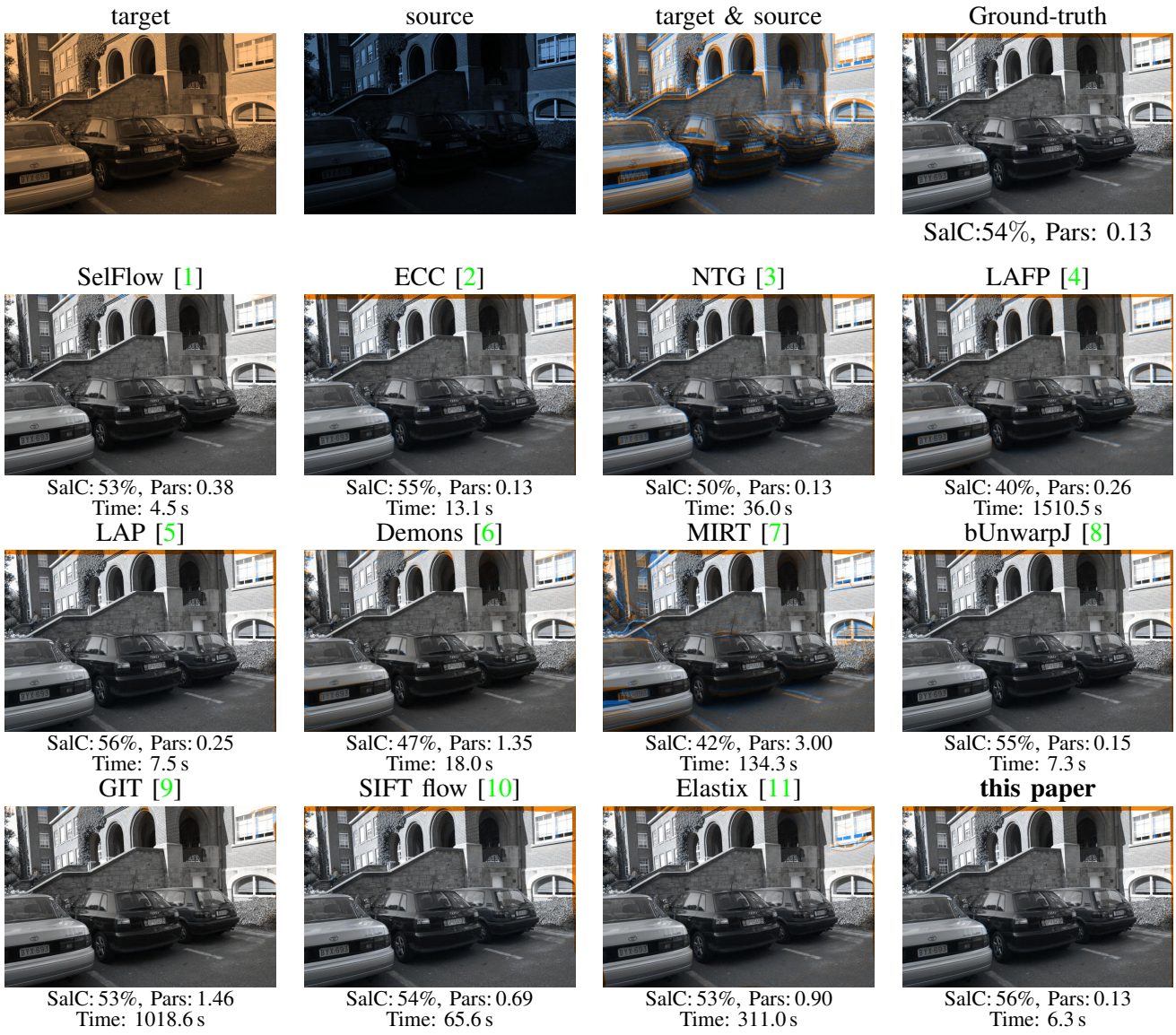

Fig. S3. Results of our algorithm on the Oxford affine dataset [12]–the subset of "Leuven" (600 × 900 pixels): alignment of the last image (i.e., the most distorted one: worst case) of each of the three subsets with the first image.

[9] S. Periaswamy and H. Farid, "Elastic registration in the presence of intensity variations," *IEEE Transactions on Medical Imaging*, vol. 22, pp. 865–874, 2003.

[10] C. Liu, J. Yuen, and A. Torralba, "SIFT flow: Dense correspondence across scenes and its applications," *IEEE Transactions on Pattern Analysis and Machine Intelligence*, vol. 33, no. 5, pp. 978–994, 2011.

[11] S. Klein, M. Staring, K. Murphy, M. A. Viergever, and J. P. Pluim, "Elastix: a toolbox for intensity-based medical image registration," *IEEE Transactions on Medical Imaging*, vol. 29, no. 1, pp. 196–205, 2010.

[12] K. Mikolajczyk, T. Tuytelaars, C. Schmid, A. Zisserman, J. Matas, F. Schaffalitzky, T. Kadir, and L. Van Gool, "A comparison of affine region detectors," *International Journal of Computer Vision*, vol. 65, no. 1-2, pp. 43–72, 2005.

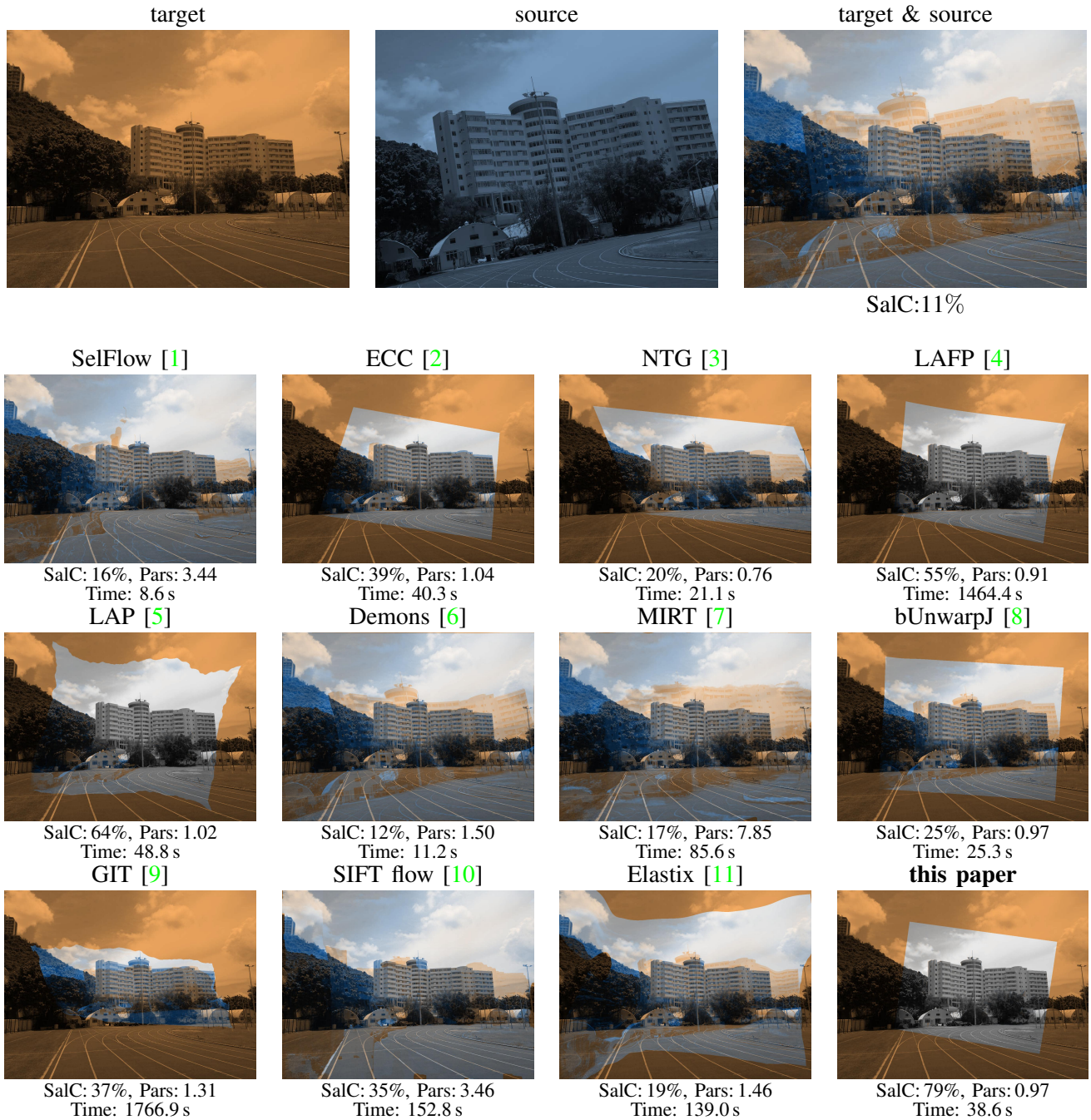

Fig. S4. Registration of real images (960 × 1280 pixels) that have undergone large rotation and scaling, using different algorithms (expanded from Fig. 8).

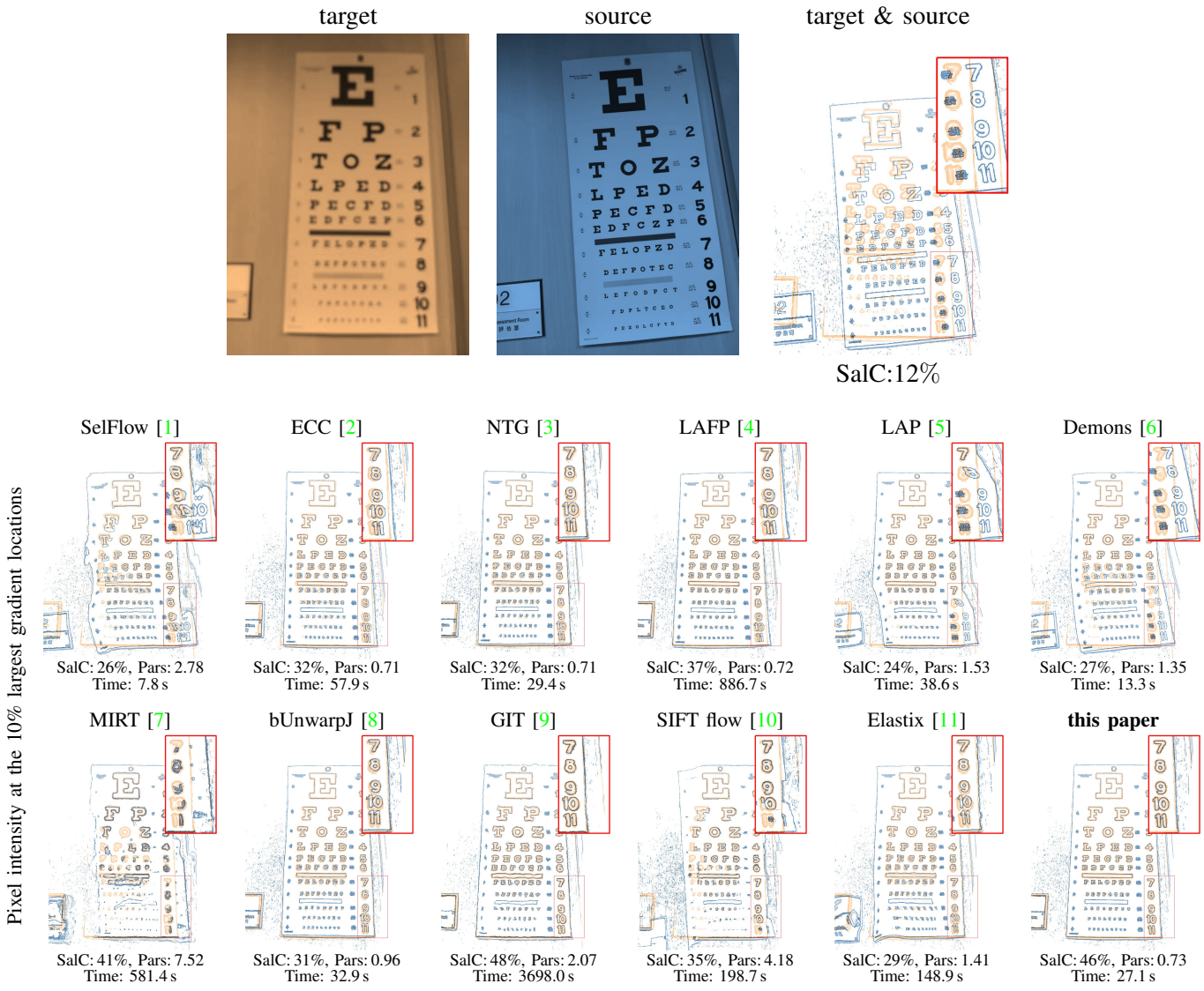

Fig. S5. Registration of real images (1440 × 1080 pixels) corrupted by blurring, using different algorithms (expanded from Fig. 9). In order to better visualise the misalignments, we outline them on the feature images.

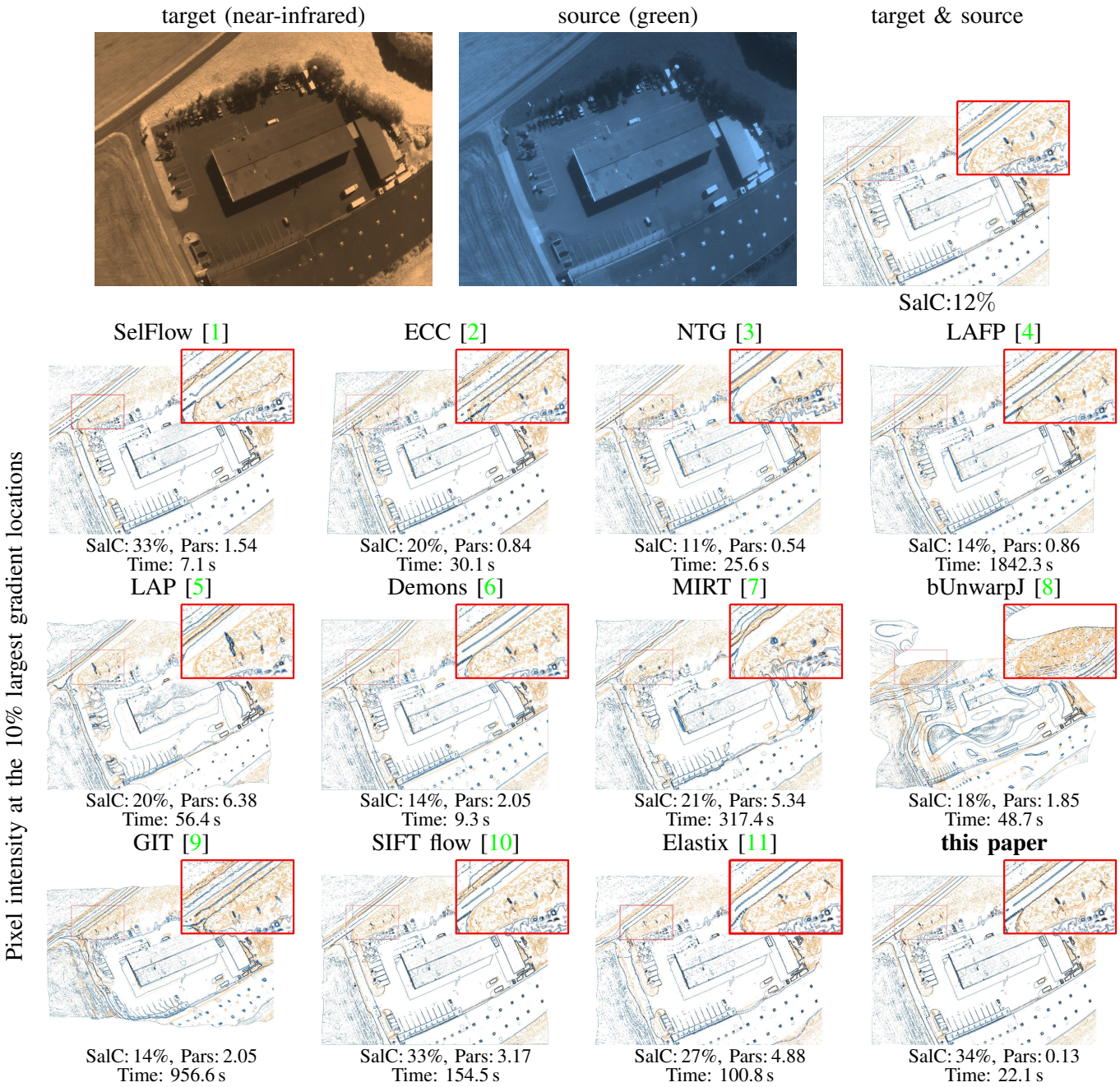

Fig. S6. Registration of multimodal satellite images (960 × 1280 pixels): overlay of the salient features (lower three rows) resulting from different algorithms (expanded from Fig. 11). The target and source images (top row) are the near-infrared and green channel of a multispectral image taken from the dataset (https://www.sensefly.com/education/datasets/).